Inorganic Chemistry

Article

pubs.acs.org/IC

Role of the Tyr-Cys Cross-link to the Active Site Properties of Galactose Oxidase

Dalia Rokhsana,[†] Alta E. Howells, David M. Dooley,*[,‡] and Robert K. Szilagyi*

Department of Chemistry and Biochemistry, Montana State University, Bozeman, Montana 59717, United States

Supporting Information

ABSTRACT: The catalytically relevant, oxidized state of the active site [Cu(II)-Y·-C] of galactose oxidase (GO) is composed of antiferromagnetically coupled Cu(II) and a post-translationally generated Tyr-Cys radical cofactor [Y·-C]. The thioether bond of the Tyr-Cys cross-link has been shown experimentally to affect the stability, the reduction potential, and the catalytic efficiency of the GO active site. However, the origin of these structural and energetic effects on the GO active site has not yet been investigated in detail. Here we present copper and sulfur K-edge X-ray absorption data and a systematic computational approach for evaluating the role of the Tyr-Cys cross-link in GO. The sulfur contribution of the Tyr-Cys cross-link to the redox active orbital is estimated from sulfur K-edge X-ray absorption spectra of oxidized GO to be about 24 ± 3%, compared to the values from computational models of apo-GO (15%) and holo-GO (22%). The results for the apo-GO computational models are in good agreement with the previously reported value for apo-GO (20 ± 3% from EPR). Surprisingly, the Tyr-Cys cross-link has only a minimal effect on the inner sphere, coordination geometry of the Cu site in the holo-protein. Its effect on the electronic structure is more striking as it facilitates the delocalization of the redox active orbital onto the thioether sulfur derived from Cys, thereby reducing the spin coupling between the [Y·-C] radical and the Cu(II) center (752 cm^{-1}) relative to the unsubstituted [Y·] radical and the Cu(II) center (2210 cm^{-1}). Energetically, the Tyr-Cys cross-link lowers the reduction potential by about 75 mV (calculated) allowing a more facile oxidation of the holo active site versus the site without the cross-link. Overall, the Tyr-Cys cross-link confers unique ground state properties on the GO active site that tunes its function in a remarkably nuanced fashion.

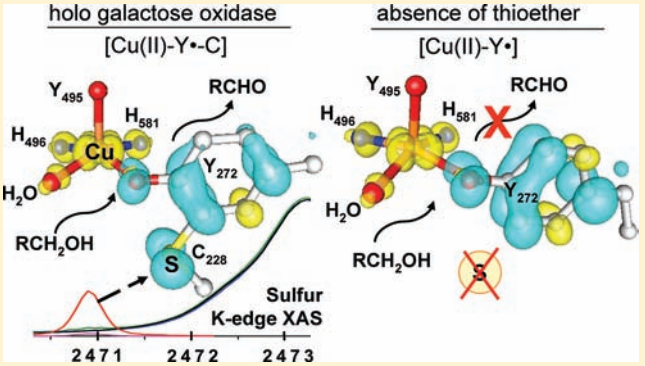

INTRODUCTION

Post-translational modifications of amino acids in proteins are ubiquitous in nature, and have been identified in many fundamental biological processes.[1] In its oxidized (reactive) state, galactose oxidase (GO) contains a Tyr-Cys radical cofactor ([Y·-C]) at its active site that is antiferromagnetically coupled to a Cu(II) ion. The Cu(II) is coordinated by two equatorial histidines, an axial tyrosine, and a water molecule, in addition to the cross-linked tyrosine (as illustrated in Figure 1). The Tyr-Cys cross-link in GO has been shown to form spontaneously on exposure to Cu(II) and dioxygen[2,3] or to excess Cu(II).[4] GO exists in three distinct oxidation states: oxidized ([Cu(II)-Y·-C]); semireduced ([Cu(II)-Y-C]); and reduced ([Cu(I)-Y-C]). The [Cu(II)-Y·-C] and the [Cu(I)-Y-C] states are involved in the catalytic cycle. The oxidized form of GO, [Cu(II)-Y·-C], catalyzes the two-electron oxidation of a broad range of primary alcohols to corresponding aldehydes with the concomitant reduction of O_2 to H_2O_2.

Atomic resolution structures of the active site for the catalytically important states are not yet available because of their inherent instability and reactivity. However, a wealth of complementary optical, magnetic, and EXAFS data for the various oxidation states of GO[5] allowed for the construction of an experimentally validated computational model of the oxidized state for the GO active site (Figures 1A and 1B).[6,7] To determine the electronic and geometric structures of the metal center and the coordinated [Y·-C] cofactor, these computational models were carefully constructed by evaluating the importance of each inner and outer sphere residue, and crystallographically resolved water molecules within approximately 12 Å of the Cu site and the Tyr-Cys cross-link. Relevant to the current study, our earlier computational studies revealed a significant amount of radical character (22 ± 2%) at the sulfur atom of the Tyr-Cys cross-link (Figure 1C).[7] Previous computational studies by others using various levels of theory and levels of truncations for model GO active sites estimated the sulfur spin density to be 6−24%.[8,9] Investigations involving biomimetic model complexes also yielded spin density distributions in this range.[9] While the lower end of this range would indicate negligible thioether sulfur contributions to the redox active orbital of the GO active site; the upper end corresponds to a remarkable electron hole delocalization that

Received: October 20, 2011
Published: February 28, 2012

   dx.doi.org/10.1021/ic2022769 | Inorg. Chem. 2012, 51, 3513−3524

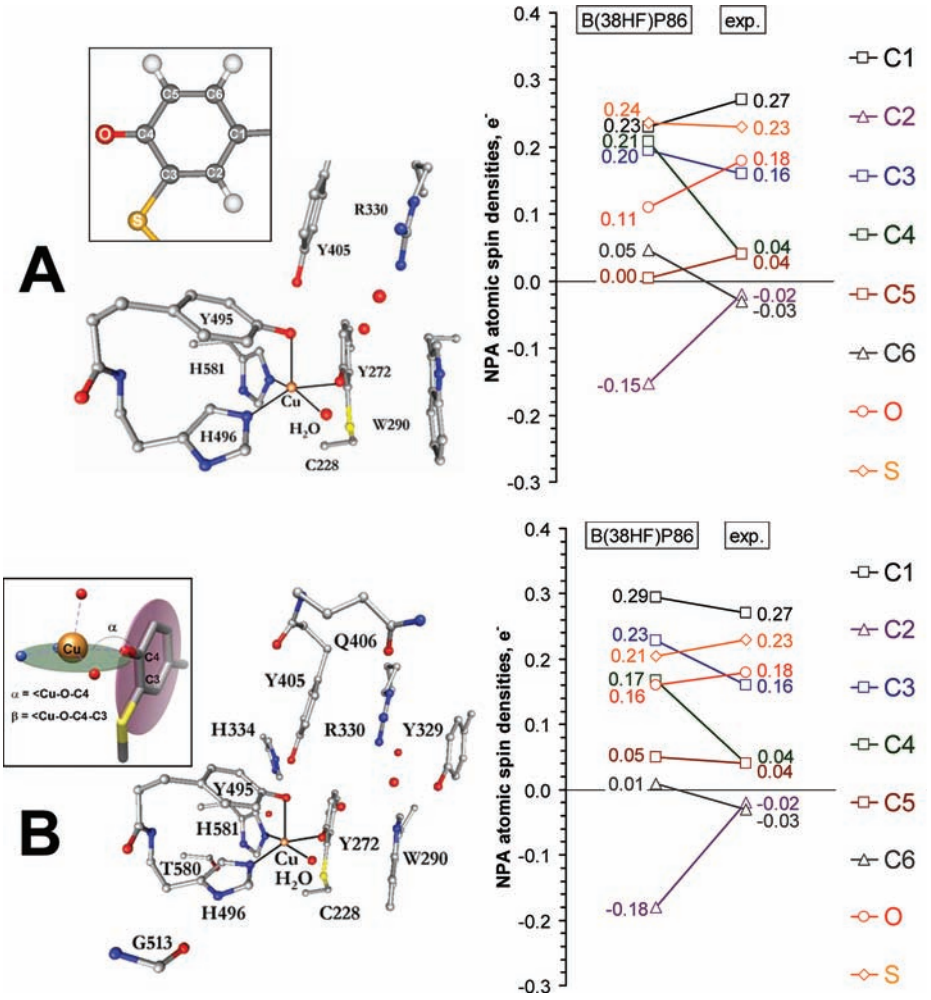

Figure 1. Optimized structures of minimal (A) and optimal (B) GO active site models along with (C) atomic spin density distributions from natural population analysis calculated at the B38HFP86/BS5 level for the Tyr-Cys cofactor in the above GO active site models. The bond angle (α = Cu−O−C4) and the dihedral angle (β = Cu−O−C4−C3) of the *xy* plane of the Cu coordination environment and Y272 ring plane are shown in the inset.

results in the appearance of about a fourth of an electron four atoms away from the Cu(II) center.

The thioether bond of the Tyr-Cys cross-link in GO has been proposed to influence both the geometric and the electronic structures of the active site. A series of site directed mutagenesis studies[10,11] clearly revealed an approximately 300 mV variability in the reduction potential for the [Y·-C]/[Y−C] pair as a function of the presence/absence of the thioether bond and the perturbation of its immediate protein environment. This is a substantial effect given that reduction potential is about 400 mV in the wild-type enzyme.[5] For example, the reduction potential in C228G variant shifts by +230 mV apparently because of the lack of the cross-link,[12] which is still much lower than that of the free tyrosyl radical (~1 V) generated in model peptides.[1] The considerable variation of reduction potentials (summarized in Supporting Information, Table S1) for a cross-linked, a coordinated, and a free Tyr, correlate with their different biochemical functions.[11] Furthermore, the electronic structure of the Tyr-Cys cross-link has also been shown to be sensitive to its environment as perturbation of the Tyr272/Trp290 π-stacking interaction in W290H increases the reduction potential by ~330 mV compared to the wild type metalloenzyme.[11]

With respect to the structural role of the Tyr-Cys cross-link, several synthetic models have already been prepared to mimic features (including the activity) of the active site of GO.[13−16] Biomimetic compounds by Tolman and Wieghardt established the importance of the coplanarity of the plane of the Cu $3d_{x^2-y^2}$ orbital and the plane of the phenolate ring, characterizing this by reference to the Cu−O−C bond angle (α), the dihedral angle of the phenolate ring, and the *xy* plane of the Cu coordination environment (β) (see inset in Figure 1B). These angles are about 129° and 75° in the crystal structure (PDB code 1GOG[17]) and 128 ± 3° and 91 ± 8° in our computational models of GO (Figures 1A and 1B) and are consistent with a diamagnetic ground state. Model complexes prepared by Stack et al.[18] show only small variations in the bond distances as a function of the three redox states and the presence of the aromatic thioether functional group, with about 300 mV variations in the reduction potential as a function of aromatic ring substituents. Facile oxidation of the tyrosine ring was observed for a unique structural model of the Cu(II) coordinated, substituted phenolate ligand,[19] where a nitro group was used to probe the effect of electron delocalization. The Cu(II) and Zn(II) complexes of Itoh et al.[17] with biologically relevant ligand environments display absorption spectra (λ_{max} = 415 and 867 nm for Cu(II)-complex and 418

dx.doi.org/10.1021/ic2022769 | Inorg. Chem. 2012, 51, 3513−3524

and 887 nm for Zn(II)-complex) that are similar to the oxidized [Cu(II)-Y·-C] form of GO (λ_{max} = 445 and 800 nm). The electron paramagnetic resonance (EPR) analysis of the $[Zn(II)(L\cdot)(NO_3)]^+$ complex (L = bis(2-pyridylethyl)(2-methylthio-4-*tert*-butyl-hydroxyphenylmethyl)amine) is consistent with significant delocalization of spin density into the methylthio group.[17] Relevant to our work, Whittaker recently determined the spin density distribution of each atom of the Tyr-Cys cross-link from a comprehensive EPR spin labeling study for the metal-free, apoenzyme, where the electron spin density on the sulfur atom is estimated to be 20 ± 3%.[20] Although qualitative trends for the roles of the Tyr-Cys cross-link are evident from the above studies, the specific relationships among structural features, the spin delocalization, variations in reduction potential, and reactivity for the Tyr-Cys unit are yet to be developed.

A direct and powerful experimental tool to examine the catalytically relevant form of GO is X-ray absorption spectroscopy (XAS) at both the S and Cu K-edges. The advantage of using this technique is that it can provide information about frontier unoccupied or redox active molecular orbitals for both diamagnetic and paramagnetic systems, while EPR technique is blind to the former. In parallel, our experimentally validated, virtual chemical model for the GO active site allowed for extensive computational studies to systematically probe (in silico mutagenesis) the roles of the Tyr-Cys thioether bond. The geometric, electronic, magnetic, and energetic contributions of the thioether bond have been determined by comparing the intact Tyr-Cys cofactor to models without the thioether bond. Herein, we report a detailed quantitative analysis of the thioether bond and its contribution to the tuning of the catalytic activity of the GO active site.

EXPERIMENTAL AND THEORETICAL METHODS

I. X-ray Absorption Measurements. *Sample Preparation.* Protein samples (~93% Cu-loaded, 3 × 150 μL, 0.633 mM protein concentration in 100 mM phosphate buffer containing 2 M urea at pH 7.0) were degassed under Ar in crimped sealed vials for 40 min on ice. Samples were oxidized and reduced with 20-fold $K_3Fe(CN)_6$ and 5 fold dithionite, respectively. Sulfur K-edge experiments were repeated with different molar ratios of protein to $K_3Fe(CN)_6$ to maximize the formation of the oxidized state of GO. The excess oxidant was removed from protein solutions by size exclusion chromatography (PD-10 from Pharmacia Biotech) under anaerobic conditions for protein concentration determination; however, for XAS measurements the excess oxidant was used to counter act photoreduction. The highest intensity S K-edge pre-edge feature was observed for the oxidized protein using 50 fold excess $K_3Fe(CN)_6$. The approximately 200 μL Delrin pinhole EXAFS cells were loaded anaerobically in an inert atmosphere glovebox after incubating the sample with oxidizing and reducing reagents for 30−40 min on ice. The samples were flash frozen and stored in liquid N_2 until the data acquisition. For XAS data renormalization, the concentration of the oxidized [Cu(II)-Y·-C] state was determined to be ~37 ± 3% in the background of semireduced [Cu(II)-Y-C] state of GO from the extinction coefficient ε = 5400 M^{-1} cm^{-1} at 445 nm and 3400 M^{-1} cm^{-1} at 800 nm.[10]

II. XAS Data Collection. Sulfur and copper K-edge XAS measurements were carried out at BL6-2 and BL7-3, respectively, at the Stanford Synchrotron Radiation Light source under storage ring (SPEAR 3) conditions of 3 GeV energy and 100−80 mA current. BL7-3 is a 20-pole, 2 T Wiggler beamline equipped with a Si(220) downward reflecting, double-crystal monochromator. Cu K-edge data were collected in the energy range of 8660−9690 eV using an unfocused beam. The frozen protein solution samples were mounted under liquid nitrogen and measured in a liquid He cryostat at about 11 K. The beamline parameters were optimized at 9685 eV. The Cu K_α fluorescence signal was collected using a 30-element Ge array detector and with a Soller slit and a Ni filter. The energy windowing of the detector was carefully done to minimize the fluorescence signal due to scattering and other non-Cu K_α emission sources. BL6-2 is a 56-pole, 0.9 T Wiggler beamline with a liquid nitrogen-cooled, Si(111) double-crystal monochromator. S K-edge spectra were collected in the energy range of 2440−2750 eV using an unfocused beam in a He-purged beam-path and an N_2-purged Lytle fluorescence detector. The beamline was optimized at 2750 eV. The protective Kapton tape was removed from the face of the EXAFS samples cells containing the frozen protein solutions under liquid nitrogen, and the cell was mounted inside a glovebag in front of a cryo-jet of liquid helium boil off to keep the sample at an approximately −180 °C. Because of the cryo-setup, no radiation damage or photoreduction was observed at either beamline (for spectral differences see Figure 3A). The incident photon energy was calibrated to the spectrum of copper foil at the Cu K-edge (first inflection point at 8979.0 eV) and the spectrum of sodium thiosulfate at the S K-edge (maximum of first pre-edge feature at 2472.0 eV).

I. Theoretical Modeling. *Computational Models.* To investigate the geometric, electronic, magnetic, and energetic role of the Tyr-Cys cross-link in the metal-free apoenzyme, several computational models were constructed from our previously reported optimal virtual chemical model of the [Cu(II)-Y·-C] state (214 atoms, Figure 1B).[7] The Cu was removed from the active site to generate the apo-model containing only the Tyr-Cys cross-link radical, [apo-Y·-C]. This model corresponds to the metalloprotein state on which the recent EPR study was conducted.[20] To compensate for the absence of the Cu(II) ion, various protonated states of the apo-model were considered with the axial Y495, or axial Y495/equatorial H496 residues being protonated in the singly [apoH$^+$-Y·-C] or the doubly protonated [apo$(H^+)_2$-Y·-C] states, respectively. The contribution of Tyr-Cys cross-link to the overall distribution of spin density is evaluated by breaking the C−S bond of the Tyr-Cys cross-link in the singly protonated apo-model [apoH$^+$-Y·-C] to obtain apo-model without the thioether bond, [apoH$^+$-Y·]. For the isolated [Y·-C] all the protein surroundings of the cross-link were deleted.

Using our converged oxidized model of the GO active site (Figure 1A), we have also evaluated the effect of the Tyr-Cys thioether bond on the geometric and the electronic structures of the native GO active site and its reduction potentials. The C−S bond of the Tyr-Cys cross-link is removed in the oxidized [Cu(II)-Y·] model, and the Cys228 residue is rotated and moved away (~3 Å) to prevent any interaction of S(Cys228) with the Tyr272 ring atoms. Semireduced [Cu(II)-Y] and reduced [Cu(I)-Y] structures without the Tyr-Cys thioether bond were obtained from a consecutive one-electron reduction of the corresponding oxidized [Cu(II)-Y·] and semireduced [Cu(II)-Y] models, respectively. To check the robustness of our computational results, semireduced [Cu(II)-Y] and reduced [Cu(I)-Y] models were also obtained from the corresponding converged computational models of the semireduced [Cu(II)-Y-C] and reduced [Cu(I)-Y-C] GO models, respectively, by removing the C−S bond and rotating the Cys residue away.

II. Density Functional Theory (DFT) Calculations. The computational approach used here is as described previously for the GO active site models[7] unless noted otherwise. Briefly, a spectroscopically calibrated, hybrid density functional [B(38HF)P86][21] is employed in our computational studies using the Gaussian03 package on a cluster of AMD Opteron 8- and 16-node servers. The triple-ζ (VTZ*)[22] and double-ζ with polarization (6-31G*)[23−25] Gaussian-type all-electron basis sets were employed in all calculations (termed BS5), which can be considered as a converged basis set for mononuclear Cu(II)-containing systems.[21,26,27] The generalized ionic fragment approach[28] is employed for reliably and reproducibly constructing the correct electronic structure for the antiferromagnetically coupled Cu(II)

dx.doi.org/10.1021/ic2022769 | Inorg. Chem. 2012, 51, 3513−3524

center and the radical Tyr-Cys ligand. Geometry optimizations were performed using spin-unrestricted calculations and maintaining the open-shell singlet or doublet spin states. During optimization, all α-carbons of the residues in the minimal and optimal holo- and apo-models were fixed at their crystallographic positions. To prevent unreasonable distortion, additional atoms of a few outer-sphere residues (R330: δN, εC, χN and W290: βC, γC) in the minimal holo-model had to be also constrained. The validation of these additional confinements has been discussed previously,[7] and the geometric and electronic structures of the active sites showed no significant changes as a result of these additional confinements. Atomic spin densities were obtained from Weinhold's Natural Population Analysis (NPA).[29−31] The strength of the antiferromagnetic coupling was determined from the energy difference between the optimized singlet and triplet states for the [Cu(II)-Y·] model using the $J{\cdot}S_1{\cdot}S_2$ Hamiltonian that gives the $\Delta E(\text{T-S}) = 2JS_{\text{Cu(II)}}{\cdot}S_{\text{[Y·-C]}}$ expression for Cu(II) and [Y·-C] two spin system, where ΔE(T-S) is the energy gap between the triplet and singlet states. Antiferromagnetic spin-coupling schemes were achieved by employing a broken symmetry approach,[32] in which the initial localized spin states were constructed by the ionic fragment approach.[28] The energies of the antiferromagnetically coupled spin states were corrected for the limitations of the broken symmetry approach in calculating true ground states for the open shell singlet states by projecting the calculated expectation value of the spin operator ($\langle S^2\rangle$) to the theoretically correct $S_t = 0$ pure ground spin state. Reduction potentials were calculated from the sum of the ionization potentials and solvent reorganization energies relative to the normal hydrogen electrode at −4.43 eV. The solvent reorganization energies were implicitly considered by polarizable continuum calculations using a solvent radius of 1.385 Å (water) and a range of dielectric constants because of the partial exposure of the active site to solvent. Bond dissociation energies (BDE) of the C−S bond of Tyr-Cys cross-link have been extensively evaluated for each GO model by formally cleaving the bond homolytically and completing the unfilled valences with two protons and electrons from various sources (H_3O^+/NHE, H_3O^+/Cu(II) and H_2O_2/O_2).

III. Ab Initio MO Calculations. To obtain a theoretically converged estimate for the atomic spin density distribution of a free [Y·-C] radical, we also carried out a series of wave function-based ab initio calculations. The reference Hartree−Fock (HF) wave function was further correlated at the MP2,[33−37] MP3,[38,39] MP4,[40] CISD,[34,41] CCSD,[42−45] and QCISD[46,47] levels. To avoid issues due to basis set insaturation using only a double-ζ quality basis set, all the ab initio molecular orbital (MO) calculations were carried out using a 6-311+G* basis set.[48−50] Owing to the strong spin polarization for the [Y·-C] radical (as manifested by the large negative atomic spin densities), we also carried out a limited inquiry into the multireference nature of the ground state electronic structure using a 9 electron/8 orbital active space, CAS(9,8).[51,52] The active space was constructed from localized Natural Bonding Orbitals (LNBOs)[31] of the HF wave function. Since the [Y·-C] radical character is expected to be present only in the out-of-plane orbitals for the planar [Y·-C] radical, the three occupied and three unoccupied localized NBOs of the tyrosine ring and the out-of-plane lone pairs of the O and the S atoms were selected for the active space. The dynamic correlation correction was calculated using the MP2 formalism (CASMP2 or CASPT2) as implemented in Gaussian093.[53,54]

IV. EPR Parameters. In addition to the atomic spin densities, we also compared the calculated g-values and hyperfine coupling constants with those from the detailed EPR study of the isotopically substituted apo-GO with the radical cross-link [Y·-C] present.[20] All combinations[55,56] of open or closed shell spin restricted or unrestricted,[57,58] spin orbit corrected, and relativistic (scalar, Pauli, or ZORA) calculations were considered[59−61] as implemented in the Amsterdam Density Functional program.[62]

RESULTS AND DISCUSSION

Near-edge X-ray Absorption Spectroscopy. The X-ray absorption spectral features below the ionization threshold of a given absorber have the potential to provide direct experimental information about orbital composition in both diamagnetic (oxidized and reduced GO) and paramagnetic (semireduced GO) states. The atomic spin density distribution from EPR measurements can be correlated with the uncompensated atomic contribution to unoccupied frontier orbitals that are probed by XAS for a given absorber. To unambiguously assess key electronic structural features among all redox states of GO and quantitatively determine the S 3p contribution to the redox active orbitals, we carried out XAS measurements at both the Cu and S K-edges.

Figure 2A compares the rising-edge features at the Cu K-edge in the three oxidation states of the GO active site. The

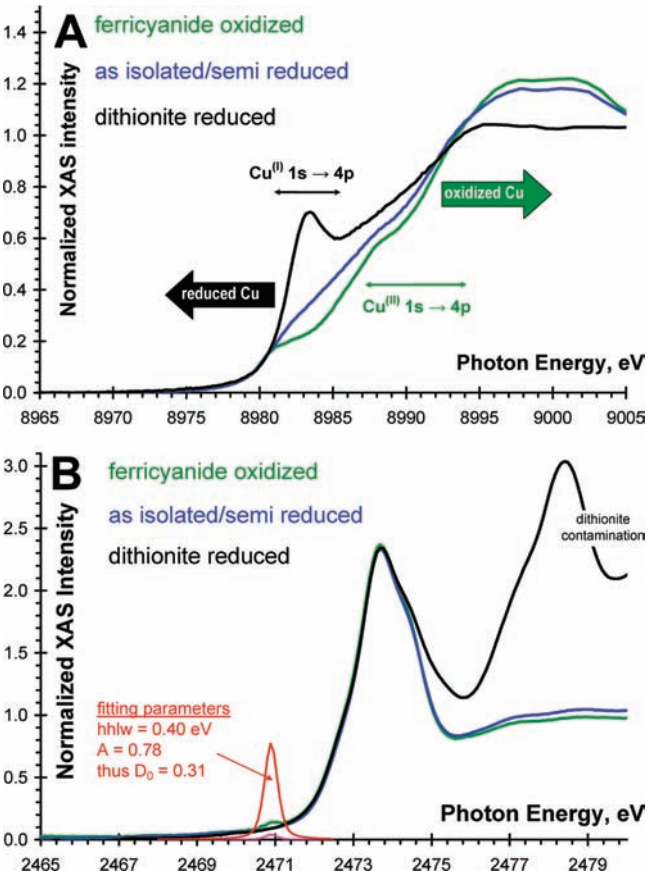

Figure 2. (A) Normalized Cu K-edge XANES data for oxidized (green), semireduced (blue), and reduced (black) form of GO. (B) Normalized S K-edge XANES data for oxidized (green), semireduced (blue), and reduced (black) form of GO. The weak peak (pink color) is obtained from the difference between the oxidized and either of the reduced spectra. The red feature is the renormalized pre-edge feature due to the presence of Tyr-Cys· in the background of 13 Met and 5 Cys that only contributes to the rising-edge and edge jump. The contamination was identified based on ref 64.

differences in rising-edge positions correlate with the Cu oxidation states between the reduced (black trace) and the oxidized (green trace) samples. Upon oxidation the Cu effective nuclear charge increases and the rising-edge features corresponding to Cu 1s→4p transitions shift to higher energies. The intense feature at 8983.5 eV corresponds to a Cu(I) 1s→$4p_z$ transition for a trigonal-planar, three coordinate Cu(I) site.[63] The intermediate energy position of the rising-edge of the semireduced form (blue trace in Figure 2A) can be

dx.doi.org/10.1021/ic2022769 | Inorg. Chem. 2012, 51, 3513−3524

rationalized by the presence of a mixture of Cu(I) and Cu(II) oxidation states. Upon isolation, dithionite reduction of the oxidized form, or oxidation of the reduced form by exposure to air, the result is always a mixture of the cuprous and cupric oxidation states with the latter being dominant. It is notable from the shoulder at 8982 eV that the oxidized form also contains a considerable amount of the reduced form. This incomplete oxidation had to be explicitly considered when the S 3p contribution from the cross-link was derived from the S K-edge data using the estimated degree of oxidation from the experimental electronic extinction coefficients.

The S K-edge XAS directly probes the electric dipole allowed S 1s→*n*p transitions. The intense line at around 2474 eV in Figure 2B[64] is due to the excitation of S 1s core electrons into the C−S σ^* orbitals of the methionine and cysteine residues. Generally, spectral features below these transitions (pre-edges) indicate the presence of unoccupied frontier orbitals with S character. No pre-edge feature is observed for both the semireduced (blue trace) and reduced (black trace) forms, while a weak pre-edge feature is detected for the oxidized form (green) at around 2471 eV. We have observed the presence of this small pre-edge feature for samples from different batches, but with varied intensities because of the difference in the Cu loading, degree of oxidation (Figure 3B). Subtraction of the

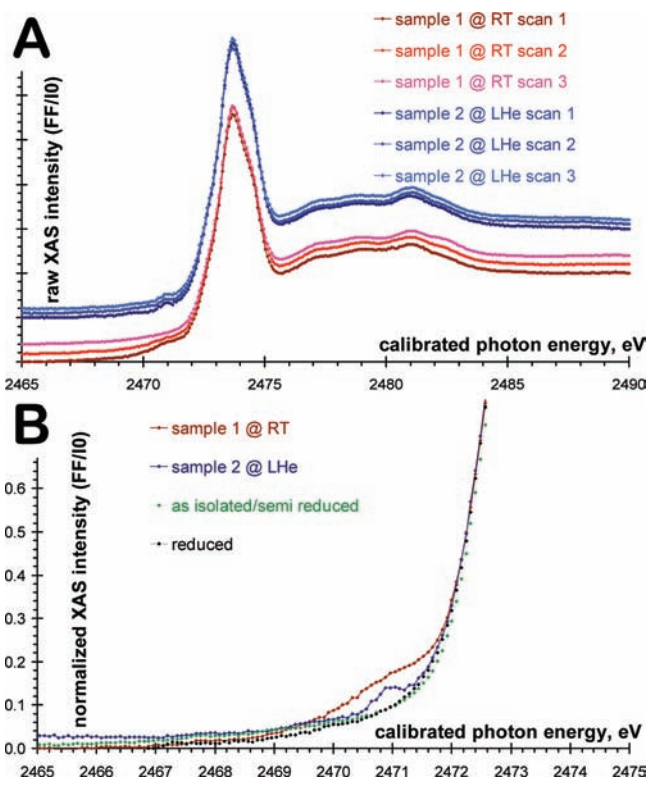

Figure 3. Representative sulfur K-edge near-edge spectra for the oxidized GO samples: (A) raw data with photoreduction for the room temperature (RT) measurements; (B) pre-edge region of the normalized data shown in Figure 2.

semireduced (blue trace) or reduced (black trace) spectra as background from the oxidized spectrum (green trace) results in a pre-edge feature (pink) shown in Figure 2B. The small intensity is due to the nineteen sulfur atoms from methionine and cysteine residues, and from disulfide bonds that contribute to the rising-edge features and to the edge-jump, while only the thioether S of the Tyr-Cys cross-link contributes to the pre-edge feature. Thus, the renormalized pre-edge feature (red) is now directly proportional to the sulfur 3p character of an electron hole associated with the Tyr-Cys thioether bond. S K-edge pre-edge features of Cu containing metalloproteins[21] are generally assigned to a direct Cu(II) and S 3p lone pair-based bond; however, no such interaction is possible for the oxidized [Cu(II)-Y··C] active site of GO. Upon one-electron reduction, this pre-edge feature disappears because of the occupation of the electron hole in the radical cross-link [Y··C]. In addition, as can be seen from the Cu K-edge spectra in Figure 2A, this reduction also partially affects the electronic structure of the Cu site, which we will elaborate below from computations.

To convert the area under a pre-edge feature (D_0) to S 3p orbital character (also commonly referred to as covalency) we need to estimate the S 1s→3p transition dipole integral for the thioether sulfur. Using the known transition dipole integrals for sulfide ($I(S^s)$ = 6.54 eV) and thiolate ($I(S^t)$ = 8.47 eV)[65] the thioether transition dipole integral, $I(S^e)$, of 10.4 eV can be estimated by assuming linear change[66] in the sulfur effective nuclear charge in going from sulfide to thiolate and to thioether. The renormalized pre-edge feature (red line in Figure 2B) can be fitted with a pseudo-Voigt line intensity of 0.309 eV. Using the $D_0 = 1/3 \cdot \alpha^2 \cdot I(S^e)$ transition dipole expression,[67] the S 3p character of 8.9% can be obtained. Correction for the partial oxidation (~37 ± 3%) increases this value to 24%. The error bar from data normalization (~7%), fitting (~5%), and concentration (~3%) of the oxidized species is estimated to be about 9%, which is only slightly worse than the typical error bars for Cu containing metalloprotein samples (~7%).[21] The large error bar is mainly because our measurements were carried out close to the detection limit of current bulk XAS data collection technique for studying a single sulfur absorber out of 19 in a protein sample with submillimolar (~600 μM) concentration. Regardless of this relatively large error bar, the pre-edge feature was always present for the oxidized Cu-bound GO samples indicating the presence of a low-lying, unoccupied orbital with non-negligible S character, as also detected independently by EPR for the Cu-free apo form of GO.

Isolated [Tyr··Cys] Cofactor. As a well-defined reference to investigate the complex structure of protein-bound Tyr-Cys cofactor, we carried out high level, systematic theoretical investigations on the isolated cross-link. We present this section separately to clearly illustrate that the potential uncertainties of computational simulations are thoroughly investigated and eliminated. Our computational models are of optimal size and include both inner and outer sphere interactions. The accuracy of the employed level of DFT has been validated by spectroscopic results and high level wave function-based methods. In our previous papers[6,7] we addressed the effect of the size of the computational model in great detail, and we only used here the structurally "converged" computational models. Here we explored the effect of various ab initio MO-, multireference active space-, and density functional-based theories on the atomic spin density distribution and spin polarization of the free [Y··C] radical.

I. Ab Initio MO-Based Electronic Structure. Taking advantage of the theoretically converging series of post-self consistent field methods, we determined the atomic spin density distribution for all the experimentally assessed atomic positions in the [Y··C] radical. The theoretical convergence corresponds to a systematically more complete treatment of electron correlation using the reference wave function defined

dx.doi.org/10.1021/ic2022769 | Inorg. Chem. 2012, 51, 3513−3524

by exact Coulomb and exchange interactions via the HF approximation. Figure 4 summarizes the atomic spin densities

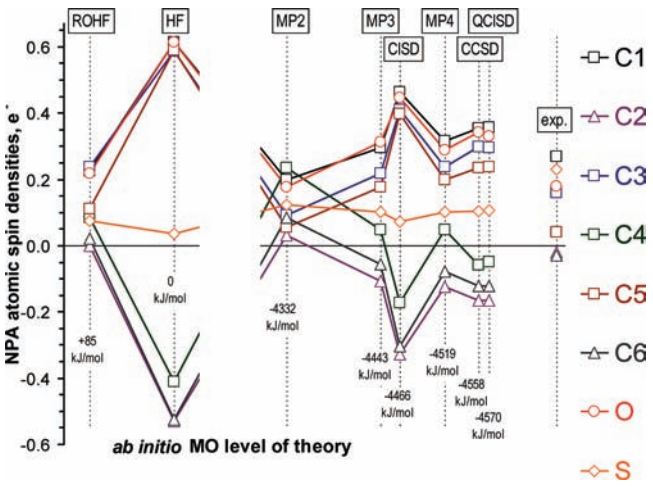

Figure 4. Ab initio wave function theory dependence of the atomic spin densities from NPA for the [Y··C] radical cofactor.

from NPA as a function of energies relative to the HF reference wave function. The basis set for all these calculations was of triple-ζ quality with additional polarization and diffuse functions. The difference in atomic spin densities between the spin-restricted (ROHF) and unrestricted (HF) open shell calculations has a considerable energetic consequence (85 kJ/mol) arising from the spin polarization, which is manifested in the appearance of large negative spin densities at positions C2 (-0.53 e$^-$), C4 (-0.41 e$^-$), and C6 (-0.52 e$^-$) of the tyrosine ring. These negative spin densities emerge from the different mixing of occupied and unoccupied orbitals within the spin-up (α) and the spin-down (β) manifold of one-electron spin orbitals. While this spin polarization disappears at the MP2 level, it is present in all unrestricted correlated and density functional calculations (vide infra). The negative spin density pattern of C2, C4, and C6 is the result of the specific mixing of the single occupied out-of-plane O lone pair with the aromatic π-system. Larger occupied π-orbital characters for positions C2, C4, and C6 are generated by the different mixing of occupied orbitals and electron holes in the β-set of the tyrosine π-orbitals (compared to the α-set) with the out-of-plane lone pairs of O and S. This in turn generates a negative spin density (as defined by the difference between α- and β-spin orbital populations), since the corresponding orbitals of the α-set will have less occupied α-orbital character for the same positions. In a spin-unrestricted UHF formalism, in contrast to a spin-restricted ROHF calculation, mixing of different orbitals is not localized solely in the singly unoccupied orbital (SUMO), but it can involve all of the symmetry allowed out-of-plane tyrosine π-orbitals, as well as O and S lone pairs. This correlates well with the configuration interaction (CI) coefficients (see below) of the complete active space (CAS) calculations.

As can be seen from the right side of Figure 4, the atomic spin density converge at the CCSD and QCISD levels to values that have a wider spread than the experimental values for the Cu-free, protein bound [Y··C] radical. The negative spin densities on the C2, C4, and C6 atoms are more negative by about 0.1−0.2 e$^-$ and the C1 and O atoms have considerably more positive values than the corresponding experimental numbers. Interestingly, the S spin density is about only half of the experimental value. However, these comparisons likely reflect potential protein environmental effects rather than the inherent accuracy of our calculations, since the experimental values are given for the protein bound [Y··C] radical. The employment of a converged level of ab initio wave function theory for realistic computational models as shown in Figure 1 is computationally prohibitive to date. On the other hand, the high level ab initio MO results can be used to evaluate the performance of various density functionals (see below), which then can be applied for computational models with hundreds of atoms.

To further probe the nature of the spin polarization in the organic [Y··C] radical, we carried out a CAS(9,8) multireference calculation. The orbitals for the active space were chosen from the localized natural bonding orbitals (Supporting Information, Figure S1). Out of the possible 3920 microstates, 14 microstates were found to contribute significantly to the ground state with more than a percent contribution. The final one-electron density matrix demonstrates the magnitude of spin polarization effects by giving 0.85, 1.00, and 1.05 e$^-$ populations for the three originally unoccupied tyrosine π*-orbitals, which in a closed shell formalism would be 2.0, 2.0, and 1.0, respectively. The diagonal value of the density matrix for the S is 1.87, which can be used to gain an estimate about the amount of spin delocalization (0.13 e$^-$). This is in good agreement with the highest level QCISD result of 0.11 e$^-$. The three most dominant microstates with more than 10% contributions in the CASMP2 calculations also show the strong spin polarization by relocating the spin α-set electrons from the lower two or three occupied to the highest two or three unoccupied orbitals of the tyrosine ring, while keeping the O lone pair and the highest tyrosine π-orbital unoccupied in the spin β-set.

II. Density Functional Theory. Figure 5 shows the atomic spin density plot as a function of the amount of HF exchange in

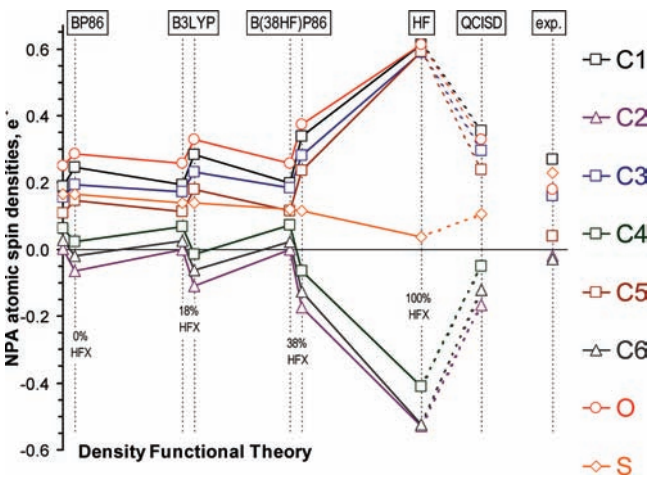

Figure 5. DFT dependence of the atomic spin densities from NPA for the [Y··C] radical cofactor.

hybrid functionals. The differences between the spin-restricted and unrestricted calculations are closely similar to that observed for the ab initio MO-based calculation; however, its energy consequence is modest (2−18 kJ/mol) relative to HF theory (85 kJ/mol). An unexpected, yet rather remarkable result from the comparison of DFT and the highest level ab initio wave function-based calculations in Figure 5 is that the spectroscopi-

dx.doi.org/10.1021/ic2022769 | Inorg. Chem. 2012, 51, 3513−3524

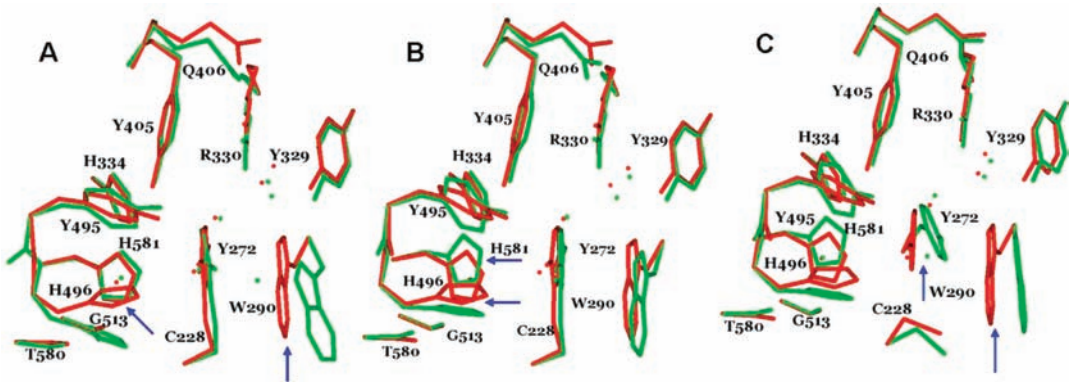

Figure 6. Overlay of initial (red) and optimized (green) geometric structures of apo-GO models: (A) apo-Y··C, (B) Y495 protonated apoH$^+$-Y··C, and (C) Y495 protonated apoH$^+$-Y· without Tyr-Cys cross-link. Large structural differences are shown with a blue arrow.

cally calibrated density functional B(38HF)P86 developed for Cu(II) complexes appears to be also the most reasonable for the organic [Y··C] radical even without the presence of a Cu(II) ion. Thus, with this comparison we eliminated the second uncertainty in modeling (see above), and this elevates the confidence of our results for the protein bound [Y··C] radical cross-link.

Since the atomic spin densities are not directly observable, we also carried out a series of density functional calculations for the EPR g-values and hyperfine coupling constants of each atom of the [Y··C] radical. Notably, regardless of the level of theory, the specific relativistic corrections, spin−orbit interactions, or the means of the population analysis employed (Mulliken or dipole derived spin densities), negative spin densities occur in these calculations as well. Surprisingly, the g-values are well reproduced (±0.01) at the pure GGA level of theory using B88 and P86 exchange and correlation functionals, respectively. From the ab initio results, we know that this agreement is fortuitous likely because of error cancellations. Using both the spin orbit interaction corrected, ZORA relativistic calculations[59−61] for open shell restricted and unrestricted with collinear approximation systems, the experimental isotropic g-value of 2.005 is reproduced with a +0.002 error. Similarly the experimental g_1, g_2, and g_3 values of 2.007, 2.006, and 2.002 were predicted to be 2.010, 2.009, and 2.002, respectively. The agreement in the hyperfine coupling constant (Supporting Information, Table S2) is less good especially with respect to the sign; however, the overall magnitude of each coupling constant is about the same as their corresponding experimental values. Overall, it appears that the fit of the multidimensional parameter space of the isotopically labeled [Y··C] radical cross-link by Whittaker[20] is robust for considering the experimental atomic spin densities from EPR to be a global minimum of the remarkable parameter space defined by the isotopic substitutions.

Protein Bound [Tyr··Cys] Cofactor. Whittaker et al. emphasized that there is a significant difference among the computationally determined and the experimentally measured electron spin densities for the Tyr-Cys cross-link.[20] The two most likely reasons for these discrepancies are the neglect of protein effect in computational models, and the shortcomings of the applied levels of theory. We have addressed the latter in the previous section. Using the virtual chemical model built for the optimal oxidized-state model shown in Figure 1B, the molecular structures and atomic spin densities for the series of apo-oxidized models in different protonation states and in the presence or absence of the Tyr-Cys cross-link were systematically evaluated as described in the Computational Models section. Thus by directly addressing two of the key issues in computational modeling, we are in the position to discuss the effects of the protein environment on the electron density distribution of the [Y··C] radical in a highly qualified manner.

I. Structural Effect of Protonation State. The removal of the active site Cu(II) ion from the oxidized holo-GO [Cu(II)-Y··C] model gives the deprotonated apo-GO model. The optimized structure of [apo-Y··C] displays large structural distortions of the first and second coordination sphere residues, H496, Y495, and W290, as shown in Figure 6A. For example, the side chain of H496 moves about 1.94 Å relative to its position in the holo-GO model. Axial Y495 shifts toward the center of the active site by about 0.33 Å measured from changes in both β- and γ-C positions of the side chain with the slight reorientation of the aromatic ring position. In addition, the Y495 residue abstracts a proton from the Y405 residue, thereby reversing the hydrogen bond donor−acceptor roles between these residues. Furthermore, the $\pi-\pi$ stacking interaction between Tyr-Cys cross-link and W290 is greatly perturbed. In the optimized structure, the β-carbon of W290 moved away by ∼1.29 Å from the stacking plane and is also rotating the entire side chain of W290. The displacement is ∼2.41 Å between the aromatic centers of W290 residues in the apo- and holo-GO models.

To compensate for the loss of the Cu(II) ion at the active site, various protonated states of apo-GO models were investigated, in part because the free tyrosinate ligand likely will be protonated at pH ∼7.0 in the apo-GO enzyme. The singly protonated state of apo-GO at Y495 [apoH$^+$-Y··C] shows a less distorted structure (Figure 6B) than the [apo-Y··C] (Figure 6A) suggesting that the introduction of a single proton can already compensate, at least in part, for the missing electrostatic interactions that are generated by the Cu(II) ion in the holo-GO model. The positions of most first and second sphere residues in the protonated apo-GO model are similar to the holo-GO model with a slight reorientation of H496, Y495, and W290 residues (Figure 6B). To compensate for the loss of Cu(II) ion in apo-GO, the doubly protonated state [apo$(H^+)_2$-Y··C] was considered where both Y495 and H496 were protonated. The doubly protonated state [apo$(H^+)_2$-Y··C] also shows a similar structure to the singly protonated [apoH$^+$-Y··C] state. The optimal pH range (6.5−7.0) for the maturation and the catalytic efficiency of GO is consistent with neutral active site histidines; hence, we use the singly protonated state

dx.doi.org/10.1021/ic2022769 | Inorg. Chem. 2012, 51, 3513−3524

[apoH$^+$-Y··C] to evaluate the role of the cross-link. The most profound effect of the elimination of the cross-link is the perturbation in the $\pi-\pi$ stacking interaction of W290 with Tyr-Cys (Figure 6C). This perturbation must be considerable, since we observe this difference despite the documented deficiencies of DFT in capturing the full effect of $\pi-\pi$ stacking and dispersion interactions.[68−72] This finding directly indicates that the presence of the Tyr-Cys thioether bond is important for maintaining the stacking interaction with W290. From previous studies, it was reported that W290 mutants affect the stability of the Tyr-Cys radical as well as the substrate binding in GO.[73] It appears that GO utilizes the unique second sphere W290 residue to protect the active site radical center, thereby stabilizing the active state and maximizing its enzymatic efficiency.

II. Effect of Protein Environment on the Spin Density Distribution of Tyr-Cys. Spin density distributions for the Tyr-Cys cross-link in apo-Y··C, apoH$^+$-Y··C, and apoH$^+$-Y· models are shown in Figure 7 with highly similar distributions for both

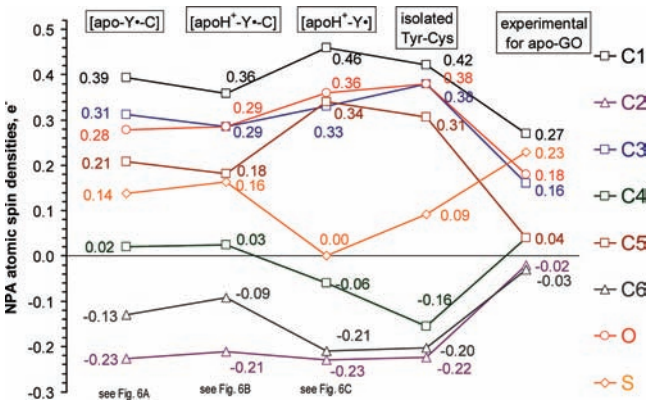

Figure 7. Spin density distribution plots of the Tyr-Cys cofactor from the apo-models in Figures 6A−C. (A) apo-Y··C, (B) Y495 protonated apoH$^+$-Y··C, and (C) Y495 protonated apoH$^+$-Y· without Tyr-Cys cross-link.

deprotonated and protonated apo-GO models. For comparison, the corresponding atomic spin densities are also shown for the isolated Tyr-Cys cross-link (see above) and the apo metalloenzyme from EPR measurements. Atomic spin densities are mainly localized at the C1, C3, and C5 positions of the tyrosine ring, and the thioether sulfur possesses 0.14−0.16 e$^-$ spin density. Notably, there is a significant difference in the spin density distribution of an isolated Tyr-Cys unit relative to its protein embedded form. The protein environment decreases the atomic spin densities on C1, C3, and C5 by 0.08−0.13 e$^-$ and makes it less negative on C2, C4, and C6 by 0.11−0.19 e$^-$. The most significant difference is at the C4 position, which changes from a negative −0.16 e$^-$ to a positive 0.02−0.03 e$^-$ value in going from the isolated [Y··C] to the protein-embedded [apo-Y··C] cross-link, respectively. This is important, since it indicates that spin polarization can be considerably influenced by a network of hydrogen bonding, dipole, and ionic interactions from the protein matrix. Contrary, the protein environment does not show any effect at the C2 position (−0.22 e$^-$ in both cases). Remarkably, the protein environment increases the spin density delocalization onto the sulfur atom by about 5−7%. This increase in spin density can be rationalized by the presence of the π-stacked W290, which benzyl ring is located above the thioether S atom of the cross-link, as non-negligible spin polarization to the order of a few percent is observed on the tryptophane's indole ring. Elimination of the cross-link (Figure 7, [apoH$^+$-Y·]) results in more polarized spin density distribution on the Tyr ring that is similar to a [Y·] radical as the sulfur spin density of 16% is redistributed over the oxygen and the carbon atoms of the Tyr ring. The spin polarization at the C3 and C5 positions adjacent to the phenolate O is actually advantageous for the regioselective formation of the cross-link with the Cys228 upon radicalization of the Tyr272 before the post-translational modification takes place. The magnitude of the calculated sulfur spin density in [apo-Y··C] is about 4−8% lower than that of the experimental spin density of apo-GO (20 ± 3% from EPR)[20] and holo-GO (24 ± 3% from S K-edge) enzymes, which is practically within the error bars of the experimental methods.

Role of the Cross-link in Oxidized-GO. To directly assess the role of the Tyr-Cys cross-link on the geometric and electronic, magnetic, and energetic properties of the catalytically relevant oxidized-GO active site, a large set of calculations were carried out using the oxidized form of the converged computational model (Figure 1A).

I. Geometric Influence. In the absence of the cross-link, the oxidized [Cu(II)-Y·], semireduced [Cu(II)-Y], and reduced [Cu(I)-Y] GO models display similar Cu coordination geometries compared to their respective models with the thioether bond intact (see Figure 8 and Supporting Information, Tables S3−S5). The oxidized [Cu(II)-Y·] state

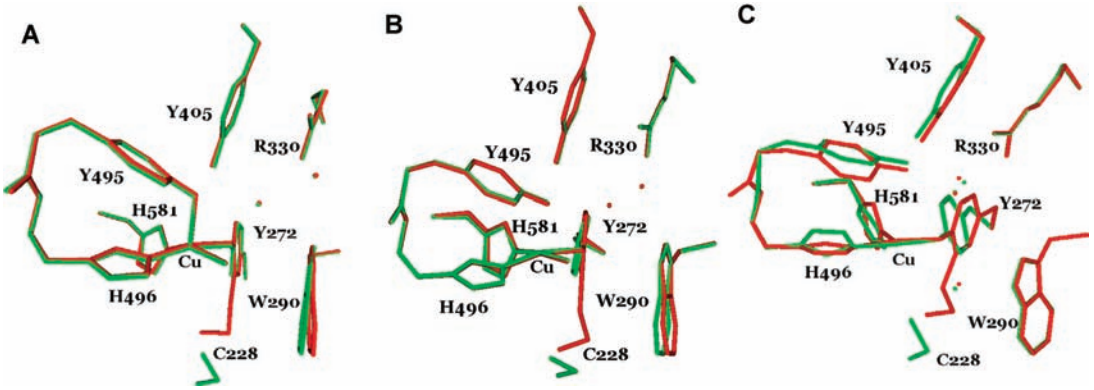

Figure 8. Overlay of optimized structures of holo-GO models in the presence (red) and absence (green) of the Tyr-Cys cross-link: (A) oxidized [Cu(II)-Y·], (B) semireduced [Cu(II)-Y], and (C) reduced [Cu(I)-Y].

dx.doi.org/10.1021/ic2022769 | Inorg. Chem. 2012, 51, 3513−3524

(Figure 8A) shows a five coordinate Cu geometry with small deviations in the Cu-L bond distances (up to 0.03 Å) and L−Cu−L bond angles (1−4°) relative to the active site [Cu(II)-Y··C] with the cross-link. The ring orientation of the tyrosine relative to the $d_{x^2-y^2}$ plane of the copper (α = 133° and β = ∼79°) is practically similar to the [Cu(II)-Y··C] model with the intact Tyr-Cys cofactor (α = 133° and β = ∼83°); hence an open shell diamagnetic electronic structure may be maintained in the absence of the thioether bond.[15] Remarkably, the key π-stacking interaction is only minimally affected in the oxidized [Cu(II)-Y·] model, whereas it was considerably perturbed in the apo-model [apo-Y·]. Thus, the Cu-bound Tyr272 in the presence of the W290 residue, but with the absence of the Tyr272-Cys228 bond (as in the C228G mutant[12]) is expected to react differently than the holo form of GO. While there is no direct experimental evidence for the existence of a Cu(II) coordinated tyrosinate anion, the presence of a Cu(I)-O(Tyr) intermediate has been assumed prior to post-translational modification.[3] The semireduced [Cu(II)-Y] structure was obtained from two different starting points; by one-electron reduction of [Cu(II)-Y·] and by eliminating the cross-link in the corresponding [Cu(II)-Y-C] model. These resulted in two stationary points with only a small energy difference of ∼4 kcal/mol for the semireduced [Cu(II)-Y] state. As observed for the oxidized model [Cu(II)-Y·], both structures show negligible changes as a result of the elimination of the Tyr-Cys cross-link with distorted tetragonal Cu coordination geometries (Figure 8B). In the reduced state, the Cu(I) ion is three-coordinate with H496, H581, and Y272 residues arranged in a trigonal planar geometry irrespective of the presence or the absence of the thioether bond (Figure 8C). There is only a little deviation in the Cu−L bond distances (up to 0.07 Å) and L−Cu−L angles (3−7°) between [Cu(I)-Y] and [Cu(I)-Y-C] models. However, the absence of the cross-link in the reduced [Cu(I)-Y] model perturbs the aromatic and imidazole ring orientation of tyrosine and histidine residues, relative to the [Cu(I)-Y-C] model. For example, the β-C of Y272 in the [Cu(I)-Y] model shifts toward the center of the active site by about 1.18 Å, which in turn tilts the aromatic ring toward the center by about 0.6−0.8 Å. Further, the side chain of Y495 shifts up by about 0.4−0.8 Å measured from changes in O, β- and γ-C (∼0.4 Å) and δ- and ε-C (∼0.8 Å) positions relative to their positions in the [Cu(I)-Y-C] model. In the presence of the cross-link, the imidazole rings of H496 and H581 are orientated parallel and perpendicular to the trigonal-plane, respectively. In the absence of the cross-link, the imidazole ring of H496 and H581 tilts up by about 22° and tilts toward the trigonal-plane by about 34° relative to the plane of [Cu(I)-Y-C], respectively (Figure 8C).

II. Electronic Influence. Despite the relatively minor impact of the thioether bond on the active-site geometry, the spin density distribution of the Tyr272 ring depends significantly on the presence of the thioether bond in the oxidized state. In a typical tyrosyl radical, electron density is localized at alternate carbon positions of the aromatic ring, C1, C3, and C5. For the optimal oxidized model [Cu(II)-Y··C], significant electron densities were calculated at C1 (0.23 e^-) and C3 (0.21 e^-), but not at C5 (0.004 e^-) positions. Interestingly, a negative spin density is only shown at the C2 position (−0.15 e^-) whereas a reverse trend is observed for the C4 (0.21 e^-) and C6 (0.05 e^-) positions in comparison to the isolated Tyr-Cys cofactor (Figure 5). The oxidized [Cu(II)-Y·] model shows significantly altered electron densities relative to [Cu(II)-Y··C]; the former are increased at C1, C3, and C5 by about 0.09−0.20 e^- and decreased at O, C4, and C6 by about 0.11−0.20 e^-. However, the electron density at the C2 position is minimally affected. These results suggest that the thioether bond plays a crucial role in the electronic structure of the Tyr-Cys unit while the geometric effect is only modest.

From the Kohn−Sham orbital analysis, the electronic transitions for the holo oxidized model were found to be at 311 and 601 nm, which were assigned as ligand-to-metal charge transfer (LMCT), from Y495 to Cu $3d_{x^2-y^2}$ orbital and ligand-to-ligand charge transfer (LLCT), tyrosinate (Y495) to tyrosyl (Y272) radical, respectively.[7] Improved agreement with the experimental electronic transitions was obtained from a time-dependent DFT (TDDFT) analysis,[7] which resulted in three strong electronic transitions at 795 nm (radical Y272 $\pi_3 \rightarrow \pi_4$), 400 nm (radical Y272 $\pi_2 \rightarrow \pi_4$), and 359 nm (H496 (π) and Y272 (π_4) to σ^* of Cu(II) $3d_{x^2-y^2}$. Elimination of the thioether bond in the holo oxidized model shifts the LLCT band from 601 to 630 nm, calculated from orbital energy differences, whereas no change is observed in the LMCT band at 311 nm. However, TDDFT results of the oxidized state without the cross-link ([Cu(II)-Y·]) show only two electronic transitions at 854 and 424 nm with significant oscillator strengths of 0.007 and 0.014, respectively. Comparable experimental electronic transitions are not available for the oxidized C228G mutant because of its higher reduction potential. However, the as-isolated C228G variant shows a band at 476 nm with a low extinction coefficient (ε = 500 M^{-1} cm^{-1}) and lacks the characteristic band of the active enzyme at 800 nm.[12] The absence of the thioether bond causes the band at 445 nm to shift by about 31 nm toward lower energy in the C228G variant of GO. In our calculation, we have also found similar changes in the electronic transitions in the presence versus absence of the thioether bond. The electronic transition at 400 nm for the [Cu(II)-Y··C] band is shifted to 424 nm for the [Cu(II)-Y·] state. However, the molecular orbitals involved in the calculated electronic transitions for [Cu(II)-Y·] are fundamentally different from those for the oxidized model with the thioether bond [Cu(II)-Y··C]. These electronic transitions can be both assigned as LLCT transitions from the π orbital of W290 to π_4 of Y272. Interestingly, there is no LMCT band found with significant oscillator strength in the TDDFT analysis. This suggests that there is a significant reorganization of the molecular orbitals in the absence of the cross-link, which explains the large effect of the thioether bond on the electronic structure (see above).

III. Magnetic Effects. The ground state of both oxidized GO forms ([Cu(II)-Y··C] or [Cu(II)-Y·]) can be characterized with an open shell, singlet spin state. The J coupling constant for [Cu(II)-Y··C] was calculated to be 752 cm^{-1}.[6] This is greatly perturbed by the absence of the thioether bond, where the coupling constant is increased by a factor of 3 (calculated: 2210 cm^{-1}). Thus, the presence of the Tyr-Cys cross-link has a profound effect on the magnetic interactions between the Cu(II) center and the Tyr-based radical. With the cross-link present, the spin density on the Tyr-Cys cofactor delocalizes to a greater extent into the peripheral atoms distant from the paramagnetic metal center, and thus reduces the magnitude of the coupling. The optimal gap between the ferro- and antiferromagnetically coupled states may have relevance to the reactivity of the GO active site. The magnitude of the singlet/triplet gap may modulate the chemical reactivity toward diamagnetic versus paramagnetic substrates, such as alcohol versus dioxygen, respectively. Also, this gap can influence the

dx.doi.org/10.1021/ic2022769 | Inorg. Chem. 2012, 51, 3513−3524

energetic of H-atom transfer processes during the catalytic cycle.

IV. Energetic Effects. Using semireduced [Cu(II)-Y] models obtained from either the one-electron reduction of [Cu(II)-Y·] and or by eliminating the cross-link in the corresponding [Cu(II)-Y-C] model, the one-electron reduction potential for the [Cu(II)-Y·]/[Cu(II)-Y] couple is calculated to be 392 or 515 mV in a dielectric constant of 40 (Supporting Information, Table S6). The negligible structural differences between the two semireduced [Cu(II)-Y] models did not allow for the exclusion of either structure; however, considering the comparable experimental reduction potential of 630 mV for the C228G variant[11] it appears that the latter is a better representation of the [Cu(II)-Y] form. The experimental reduction potential of the C228G is about 230 mV greater relative to the wild-type holo-GO, which is qualitatively well reproduced by the calculated 76 mV shift for the [Cu(II)-Y·]/[Cu(II)-Y] couple relative to the previously calculated value for holo-GO [Cu(II)-Y·-C]/[Cu(II)-Y-C] couple of 439 mV.[7] The reproduction of small energetic differences of about 150 mV is challenging for DFT without the explicit consideration of charged residues and dipoles from the rest of a larger protein environment than that considered in the given study. The more positive reduction potential in the absence of the thioether bond indicates that active site oxidation is more difficult than in the catalytically active form of GO. In the absence of the cross-link [Cu(II)-Y], the active site is harder to oxidize; hence, the formation of the diradical state, which facilitates H-atom transfer from the alcohol substrate, is less likely than for [Cu(II)-Y-C].

The C−S bond dissociation energy (BDE) of the thioether bond in the Tyr-Cys cross-link for [Cu(II)-Y·-C] was estimated using the following equation:

$$\text{Cu(II)-Tyr·-S-Cys} + \text{H}_2\text{O}_2 \rightarrow \text{Cu(II)-Tyr·-H} + \text{H-S-Cys} + \text{O}_2 \quad (1)$$

The energetic cost of C−S bond dissociation using all three holo-GO models ([Cu(II)-Y·-C], [Cu(II)-Y-C], and [Cu(I)-Y-C]) is calculated to be ∼33 ± 2 kcal/mol using the proton and electron source from solvated $H_2O_2·4H_2O$ (Supporting Information, Table S7).[74] Calculation of the direct, homolytic cleavage energy of the C−S bond in the reduced [Cu(I)-Y-C] model to give [Cu(I)-Y· + ·C] resulted in bond dissociation energy of 72 kcal/mol, similar to the reported literature value of 61 kcal/mol for the C−S bond dissociation energy in $PhCH_2$−S-CH_3.[75] The substantial bond formation energy of the C−S bond produced in the self-processing post-translational modification reaction may provide considerable stabilization of the active site of GO, which is subsequently exploited in the catalysis of alcohol oxidation.

CONCLUSIONS AND MECHANISTIC ROLE OF TYR-CYS

The presence of the Tyr-Cys cross-link has been shown earlier to affect the radical stability and catalytic efficiency of galactose oxidase.[12] In this paper, we have specifically addressed the role of the thioether bond formed in a post-translational modification upon the first turnover of the GO active site between the spatially adjacent Tyr272 and Cys228 on the electronic and geometric structures of the GO active site, and on the overall stability and reactivity of this novel site. Importantly, our spectroscopic and computational results directly establish the magnitude of the spin delocalization on the thioether sulfur atom in the catalytically critical [Cu(II)-Y·-C] state, as a key electronic structural feature related to the active site redox chemistry. To ensure the reliability of our computed atomic spin densities, a systematically converging set of ab initio wave function-based methods validated the Tyr-Cys radical spin density from hybrid DFT calculations. We confirmed the adequacy of our computational level of theory by obtaining practically identical results by the highest level of ab initio wave function-based method (QCISD) and our preferred hybrid DFT functional (B38HFP86). Thus, we were able to provide a comprehensive evaluation of the role of the Tyr-Cys cross-link via a thorough electronic and geometric structure modeling.

Specific geometric, electronic, magnetic, and energetic effects were elucidated for the thioether bond in the Tyr-Cys active-site unit, which confers the unique ground state properties on the active site of GO. Our computational work shows that the ground state of the GO active site is fine-tuned toward optimal reactivity. The Cu(II) ligands and a small outer sphere environment from protein side chains and solvent molecules affect the geometric structure, the nature of the redox active orbitals, and the reduction potentials. One might have expected that the presence or absence of a C−S bond between residues separated by more than 50 amino acids that would normally not even get involved in a weak interaction (C−H and H−S bonds), would lead to structural perturbation around a metalloenzyme active site between the holo and the apo forms. Remarkably, this is not the case for GO. The modest structural effects of the Cu coordination environment upon elimination of the cross-link parallels the observations made by Stack et al.[16] for synthetic models that show only small variation in the Cu-ligand bond distances as a function of redox states as well as the presence or absence of the aromatic thioether functional group. This can be rationalized by reference to the nature of the bonding interactions at the GO active site. The Cu $3d_{x^2-y^2}$ and the coupled O(Tyr) lone pair of the σ interaction are practically orthogonal to the Tyr radical out-of-plane orbitals of the π interaction. Only the latter are responsible for the electronic coupling to the thioether S lone pair. Thus, because of this orthogonality, the thioether bond will have only limited effect on the Cu-based metal−ligand interactions. Contrary, the lack of the Tyr-Cys cross-link shows remarkable structural changes for the π-stacking interaction between the Cu-bound Tyr272 and W290 residues in the apo-GO form. This observation suggests that upon Cu(II) binding its coordination environment becomes tightly packed and actually the presence of the π-stacking tryptophan residue is more influential in determining the active site geometry than the cross-link.

Furthermore, the electronic structure differences tell a different story. The cross-link allows for electron delocalization onto S(Cys) (exp: 20 ± 3% from EPR, 24 ± 3% from S K-edge, and calc: 15 ± 1% for apo-GO and 22 ± 2% for holo-GO models), making the Tyr-Cys radical less strongly coupled (J = 752 cm^{-1}) than a Tyr radical (J = 2210 cm^{-1}) to the Cu(II) center. This may rationalize why the Tyr-Cys cofactor can act as an independent redox center next to a Cu(II) site during hydrogen atom abstraction from the alcohol during the catalytic cycle. In addition, the presence of the cross-link lowers the reduction potential by about 75 mV (calculated) and 230 mV (experimental from C228G variant) relative to the active site without the cross-link. Although this is numerically a small

dx.doi.org/10.1021/ic2022769 | Inorg. Chem. 2012, 51, 3513−3524

difference, it appears to be sufficient to modulate the reactivity of Tyr272, such that the activated C−H bond of the alcohol substrate is attacked preferentially. We found evidence from our calculations for the role of the cross-link sulfur to mediate steric and electronic effects of the W290 residue from the second sphere protein environment via covalent interactions as indicated by the non-negligible sulfur atomic spin density distribution.

We can conclude that the presence of the cross-link embedded in an appropriate protein environment is essential in fine-tuning the electronic structure of the GO active site toward performing a two-electron oxidation of alcohols efficiently versus a two-electron, mononuclear radical substitution (S_R1) reaction. The latter; however, is required in the post-translational modification to actually create the catalytically active site with the Tyr-Cys cross-link.

■ ASSOCIATED CONTENT

Supporting Information

Optimized coordinates, structural comparison of GO models in the presence or absence of the cross-link, reduction potential calculation, compilation of experimental reduction potentials, bond dissociation energy, MO of isolated Tyr-Cys. This material is available free of charge via the Internet at http://pubs.acs.org. Further supporting information with formatted Gaussian checkpoint files, fragment files used for merging electronic structures from ionic fragments can be found at http://computational.chemistry.montana.edu/SI.

■ AUTHOR INFORMATION

Corresponding Author

*E-mail: davedooley@uri.edu (D.M.D.), szilagyi@montana.edu (R.K.S.).

Present Addresses

[†]Department of Chemistry, Whitman College, Hall of Science, Walla Walla, WA 99362.

[‡]The University of Rhode Island, Green Hall, 35 Campus Avenue, Kingston, RI 02881.

Notes

The authors declare no competing financial interest.

■ ACKNOWLEDGMENTS

We greatly acknowledge the support of this research from the National Institute of Health (GM 27659 to D.M.D) and from the National Science Foundation (0744820 to R.K.S). Portions of this research were carried out at the Stanford Synchrotron Radiation Lightsource, a Directorate of SLAC National Accelerator Laboratory and an Office of Science User Facility operated for the U.S. Department of Energy Office of Science by Stanford University. The SSRL Structural Molecular Biology Program is supported by the DOE Office of Biological and Environmental Research, and by the National Institutes of Health, National Center for Research Resources, Biomedical Technology Program (P41RR001209).

■ REFERENCES

(1) Stubbe, J. A.; van der Donk, W. A. *Chem. Rev.* **1998**, *98* (7), 2661−2661.

(2) Rogers, M. S.; Baron, A. J.; McPherson, M. J.; Knowles, P. F.; Dooley, D. M. *J. Am. Chem. Soc.* **2000**, *122* (5), 990−991.

(3) Whittaker, M. M.; Whittaker, J. W. *J. Biol. Chem.* **2003**, *278* (24), 22090−22101.

(4) Rogers, M. S.; Hurtado-Guerrero, R.; Firbank, S. J.; Halcrow, M. A.; Dooley, D. M.; Phillips, S. E. V.; Knowles, P. F.; McPherson, M. J. *Biochemistry* **2008**, *47* (39), 10428−10439.

(5) Whittaker, J. W. *Chem. Rev.* **2003**, *103* (6), 2347−2363.

(6) Rokhsana, D.; Dooley, D. M.; Szilagyi, R. K. *J. Am. Chem. Soc.* **2006**, *128* (49), 15550−15551.

(7) Rokhsana, D.; Dooley, D. M.; Szilagyi, R. K. *J. Biol. Inorg. Chem.* **2008**, *13* (3), 371−383.

(8) Himo, F.; Eriksson, L. A.; Maseras, F.; Siegbahn, P. E. M. *J. Am. Chem. Soc.* **2000**, *122* (33), 8031−8036.

(9) Rothlisberger, U.; Carloni, P.; Doclo, K.; Parrinello, M. *J. Biol. Inorg. Chem.* **2000**, *5* (2), 236−250.

(10) Whittaker, M. M.; Whittaker, J. W. *J. Biol. Chem.* **1988**, *263* (13), 6074−6080.

(11) Wright, C.; Sykes, A. G. *J. Inorg. Biochem.* **2001**, *85* (4), 237−243.

(12) Baron, A. J.; Stevens, C.; Wilmot, C.; Seneviratne, K. D.; Blakeley, V.; Dooley, D. M.; Phillips, S. E. V.; Knowles, P. F.; McPherson, M. J. *J. Biol. Chem.* **1994**, *269* (40), 25095−25105.

(13) Chaudhuri, P.; Hess, M.; Muller, J.; Hildenbrand, K.; Bill, E.; Weyhermuller, T.; Wieghardt, K. *J. Am. Chem. Soc.* **1999**, *121* (41), 9599−9610.

(14) Halfen, J. A.; Young, V. G.; Tolman, W. B. *Angew. Chem., Int. Ed. Engl.* **1996**, *35* (15), 1687−1690.

(15) Muller, J.; Weyhermuller, T.; Bill, E.; Hildebrandt, P.; Ould-Moussa, L.; Glaser, T.; Wieghardt, K. *Angew. Chem., Int. Ed.* **1998**, *37* (5), 616−619.

(16) Pratt, R. C.; Stack, T. D. P. *Inorg. Chem.* **2005**, *44* (7), 2367−2375.

(17) Itoh, S.; Taki, M.; Takayama, S.; Nagatomo, S.; Kitagawa, T.; Sakurada, N.; Arakawa, R.; Fukuzumi, S. *Angew. Chem., Int. Ed.* **1999**, *38* (18), 2774−2776.

(18) Wang, Y. D.; DuBois, J. L.; Hedman, B.; Hodgson, K. O.; Stack, T. D. P. *Science* **1998**, *279* (5350), 537−540.

(19) Thomas, F.; Gellon, G.; Luneau, I. G.; Saint-Aman, E.; Pierre, J. L. *Angew. Chem., Int. Ed.* **2002**, *41* (16), 3047−3050.

(20) Lee, Y. K.; Whittaker, M. M.; Whittaker, J. W. *Biochemistry* **2008**, *47* (25), 6637−6649.

(21) Szilagyi, R. K.; Metz, M.; Solomon, E. I. *J. Phys. Chem. A* **2002**, *106* (12), 2994−3007.

(22) Schafer, A.; Horn, H.; Ahlrichs, R. *J. Chem. Phys.* **1992**, *97* (4), 2571−2577.

(23) Harihara, Pc; Pople, J. A. *Theor. Chim. Acta* **1973**, *28* (3), 213−222.

(24) Francl, M. M.; Pietro, W. J.; Hehre, W. J.; Binkley, J. S.; Gordon, M. S.; Defrees, D. J.; Pople, J. A. *J. Chem. Phys.* **1982**, *77* (7), 3654−3665.

(25) Rassolov, V. A.; Pople, J. A.; Ratner, M. A.; Windus, T. L. *J. Chem. Phys.* **1998**, *109* (4), 1223−1229.

(26) Ryde, U.; Olsson, M. H. M.; Pierloot, K. The structure and function of blue copper proteins. In *Theoretical Biochemistry. Processes and properties of biological systems*; Eriksson, L. A., Ed.; Elsevier: Amsterdam, The Netherlands, 2001; Vol. 9, pp 1−56.

(27) Siegbahn, P. E. M.; Blomberg, M. R. A. *Chem. Rev.* **2000**, *100* (2), 421−437.

(28) Szilagyi, R. K.; Winslow, M. A. *J. Comput. Chem.* **2006**, *27* (12), 1385−1397.

(29) Reed, A. E.; Curtiss, L. A.; Weinhold, F. *Chem. Rev.* **1988**, *88* (6), 899−926.

(30) Foster, J. P.; Weinhold, F. *J. Am. Chem. Soc.* **1980**, *102* (24), 7211−7218.

(31) Weinhold, F. Natural Bond Orbital Methods. In *Encyclopedia of Computational Chemistry*; Allinger, N. L.; Schaefer III, H. F.; Clark, T.; Gasteiger, J.; Kollman, P.; Schreiner, P., Eds.; John Wiley & Sons: Chichester, U.K., 2002; Vol. 3, pp 1792−1811.

(32) Clark, A. E.; Davidson, E. R. *J. Chem. Phys.* **2001**, *115* (16), 7382−7392.

(33) Saebo, S.; Almlof, J. *Chem. Phys. Lett.* **1989**, *154* (1), 83−89.

(34) Head-Gordon, M.; Head-Gordon, T. *Chem. Phys. Lett.* **1994**, *220* (1−2), 122−128.
(35) Frisch, M. J.; Head-Gordon, M.; Pople, J. A. *Chem. Phys. Lett.* **1990**, *166* (3), 281−289.
(36) Frisch, M. J.; Head-Gordon, M.; Pople, J. A. *Chem. Phys. Lett.* **1990**, *166* (3), 275−280.
(37) Head-Gordon, M.; Pople, J. A.; Frisch, M. J. *Chem. Phys. Lett.* **1988**, *153* (6), 503−506.
(38) Pople, J. A.; Binkley, J. S.; Seeger, R. *Int. J. Quantum Chem.* **1976**, 1−19.
(39) Pople, J. A.; Seeger, R.; Krishnan, R. *Int. J. Quantum Chem.* **1977**, 149−163.
(40) Krishnan, R.; Pople, J. A. *Int. J. Quantum Chem.* **1978**, *14* (1), 91−100.
(41) Head-Gordon, M.; Maurice, D.; Oumi, M. *Chem. Phys. Lett.* **1995**, *246* (1−2), 114−121.
(42) Scuseria, G. E.; Schaefer, H. F. *J. Chem. Phys.* **1989**, *90* (7), 3700−3703.
(43) Scuseria, G. E.; Janssen, C. L.; Schaefer, H. F. *J. Chem. Phys.* **1988**, *89* (12), 7382−7387.
(44) Purvis, G. D.; Bartlett, R. J. *J. Chem. Phys.* **1982**, *76* (4), 1910−1918.
(45) Čížek, J. On the Use of the Cluster Expansion and the Technique of Diagrams in Calculations of Correlation Effects in Atoms and Molecules. In *Correlation Effects in Atoms and Molecules*; LeFebvre, R., Moser, C., Eds.; John Wiley & Sons, Inc.: New York, 1969; Vol. *9*, pp 35−89.
(46) Salter, E. A.; Trucks, G. W.; Bartlett, R. J. *J. Chem. Phys.* **1989**, *90* (3), 1752−1766.
(47) Gauss, J.; Cremer, D. *Chem. Phys. Lett.* **1988**, *150* (3−4), 280−286.
(48) Raghavachari, K.; Trucks, G. W. *J. Chem. Phys.* **1989**, *91* (2), 1062−1065.
(49) Hay, P. J. *J. Chem. Phys.* **1977**, *66* (10), 4377−4384.
(50) Wachters, A. J. *J. Chem. Phys.* **1970**, *52* (3), 1033.
(51) Frisch, M.; Ragazos, I. N.; Robb, M. A.; Schlegel, H. B. *Chem. Phys. Lett.* **1992**, *189* (6), 524−528.
(52) Schlegel, H. B.; Robb, M. A. *Chem. Phys. Lett.* **1982**, *93* (1), 43−46.
(53) Tonachini, G.; Schlegel, H. B.; Bernardi, F.; Robb, M. A. *J. Am. Chem. Soc.* **1990**, *112* (2), 483−491.
(54) Bernardi, F.; Bottoni, A.; Field, M. J.; Guest, M. F.; Hillier, I. H.; Robb, M. A.; Venturini, A. *J. Am. Chem. Soc.* **1988**, *110* (10), 3050−3055.
(55) van Lenthe, E.; Wormer, P. E. S.; vanderAvoird, A. *J. Chem. Phys.* **1997**, *107* (7), 2488−2498.
(56) van Lenthe, E.; van der Avoird, A.; Wormer, P. E. S. *J. Chem. Phys.* **1998**, *108* (12), 4783−4796.
(57) Patchkovskii, S.; Ziegler, T. *J. Phys. Chem. A* **2001**, *105* (22), 5490−5497.
(58) Schreckenbach, G.; Ziegler, T. *J. Phys. Chem. A* **1997**, *101* (18), 3388−3399.
(59) Patchkovskii, S.; Strong, R. T.; Pickard, C. J.; Un, S. *J. Chem. Phys.* **2005**, *122* (21), 214101.
(60) Patchkovskii, S.; Schreckenbach, G. Calculation of EPR g-Tensors with Density Functional Theory. In *Calculation of NMR and EPR Parameters: Theory and Applications*; Kaupp, M., Bühl, M., Malkin, V. G., Eds.; Wiley-VCH Verlag GmbH & Co. KGaA: Weinheim, Germany, 2004; Vol. *32*.
(61) Pickard, C. J.; Mauri, F. *Phys. Rev. Lett.* **2002**, *88* (8), 086403.
(62) Velde, G. T.; Bickelhaupt, F. M.; Baerends, E. J.; Guerra, C. F.; Van Gisbergen, S. J. A.; Snijders, J. G.; Ziegler, T. *J. Comput. Chem.* **2001**, *22* (9), 931−967.
(63) Kau, L. S.; Spirasolomon, D. J.; Pennerhahn, J. E.; Hodgson, K. O.; Solomon, E. I. *J. Am. Chem. Soc.* **1987**, *109* (21), 6433−6442.
(64) Hedman, B.; Frank, P.; Gheller, S. F.; Roe, A. L.; Newton, W. E.; Hodgson, K. O. *J. Am. Chem. Soc.* **1988**, *110* (12), 3798−3805.
(65) Sarangi, R.; George, S. D.; Rudd, D. J.; Szilagyi, R. K.; Ribas, X.; Rovira, C.; Almeida, M.; Hodgson, K. O.; Hedman, B.; Solomon, E. I. *J. Am. Chem. Soc.* **2007**, *129* (8), 2316−2326.
(66) Shadle, S. E.; Hedman, B.; Hodgson, K. O.; Solomon, E. I. *J. Am. Chem. Soc.* **1995**, *117* (8), 2259−2272.
(67) Hedman, B.; Hodgson, K. O.; Solomon, E. I. *J. Am. Chem. Soc.* **1990**, *112* (4), 1643−1645.
(68) Zhao, Y.; Truhlar, D. G. *J. Chem. Theory Comput.* **2007**, *3* (1), 289−300.
(69) Schwabe, T.; Grimme, S. *Acc. Chem. Res.* **2008**, *41* (4), 569−579.
(70) Johnson, E. R.; Mackie, I. D.; DiLabio, G. A. *J. Phys. Org. Chem.* **2009**, *22* (12), 1127−1135.
(71) Guerra, C. F.; van der Wijst, T.; Poater, J.; Swart, M.; Bickelhaupt, F. M. *Theor. Chem. Acc.* **2010**, *125* (3−6), 245−252.
(72) Grimme, S.; Antony, J.; Schwabe, T.; Muck-Lichtenfeld, C. *Org. Biomol. Chem.* **2007**, *5* (5), 741−758.
(73) Rogers, M. S.; Tyler, E. M.; Akyumani, N.; Kurtis, C. R.; Spooner, R. K.; Deacon, S. E.; Tamber, S.; Firbank, S. J.; Mahmoud, K.; Knowles, P. F.; Phillips, S. E. V.; McPherson, M. J.; Dooley, D. M. *Biochemistry* **2007**, *46* (15), 4606−4618.
(74) Rokhsana, D. It is important to emphasize that the C-S bond dissociation energy (BDE(C-S)) is sensitive to the selected proton and the electron sources. For example, using the combinations of $H_3O^+ \cdot 4H_2O$/NHE or $H_3O^+ \cdot 4H_2O$/Cu(I) the BDE(C-S) are calculated to be 2 and −16 kcal/mol, respectively . 2011.
(75) Colussi, A. J.; Benson, S. W. *Int. J. Chem. Kinet.* **1977**, *9* (2), 307−316.